atmosphere

MDPI

Article

Effect of Spatial Variation of Convective Adjustment Time on the Madden–Julian Oscillation: A Theoretical Model Analysis

Hui Wang [1], Yuntao Wei [2,3] and Fei Liu [1,*]

[1] Earth System Modeling Center and climate dynamics research center, Nanjing University of Information Science and Technology, Nanjing 210044, China; wanghui_ld@126.com
[2] Key Laboratory of Ocean Circulation and Waves, Institute of Oceanology, Chinese Academy of Sciences, Qingdao 266071, China; weiyuntaowyt@163.com
[3] University of Chinese Academy of Sciences, Beijing 100049, China
* Correspondence: liuf@nuist.edu.cn

Received: 29 August 2017; Accepted: 17 October 2017; Published: 20 October 2017

Abstract: The observed convective adjustment time (CAT) associated with Madden–Julian Oscillation (MJO) precipitation is found to vary significantly in space. Here, we investigate the effect of different spatial distributions of CAT on MJO precipitation based on the frictional coupled dynamics moisture (FCDM) model. The results show that a large value of CAT tends to decrease the frequency and growth rate of eastward-propagating MJO-like mode in the FCDM model, delaying the occurrence of MJO deep convection and slowing down its eastward propagation. A large phase lag between circulation and convection decreases convective available potential energy (CAPE). In the observations, a small background vertical moisture gradient (BVMG) tends to increase the frequency associated with cold sea surface temperature (SST), while a large value of CAT tends to decrease the frequency. Due to their competing effect, the simulated frequency and phase speed remain the same when the convection moves from a warm to a cold SST region. The convection is heavily suppressed over the cold SST region due to the decreasing growth rate of unstable wavenumber-one mode with smaller BVMG and longer CAT. This theoretical finding should improve our understanding of MJO dynamics and simulation.

Keywords: Madden–Julian Oscillation; convective adjustment time; convective relaxation frequency; spatial variation; frictionally coupled dynamics moisture model

1. Introduction

The Madden–Julian Oscillation (MJO) is the dominant intraseasonal oscillation in the tropical atmosphere with a broad period from 30 to 90 days [1,2]. The MJO provides a major predictability source for extended-range weather forecasting, which bridges traditional weather forcast and modern-day climate prediction [3,4]. In spite of this importance [5,6], explicit MJO simulation in state-of-the-art general circulation models (GCMs) is still far from satisfactory [7].

After decades of research, our understanding of the MJO has advanced greatly. The conditional instability of the second kind (CISK) [8] and wave-CISK [9] theories were used to explain the MJO instability, while the instability is the greatest at the smallest scales [10,11]. This CISK instability was found to be unphysical [12] and cannot support the MJO growth in GCMs [13]. The frictional planetary boundary layer (PBL) moisture convergence was then found to provide an instability source for the planetary-scale MJO [14]. Kelvin–Rossby wave dynamics from the equatorial wave theory [15,16] together with frictional boundary layer processes have been used to explain the horizontal structure, leading vertical moisture advection to the east, and selected eastward propagation

of the MJO [14,17–19]. Another advancement includes improving our understanding of moist static energy variation of the MJO; the "moisture mode" theory focuses on moisture processes of the MJO [20,21], in which cloud-radiation interaction and wind-induced surface heat exchange (WISHE) provide an instability source to destabilize the "moisture mode" against atmospheric dissipation [22,23], and the horizontal moisture advection of the seasonal mean moisture by anomalous wind of the MJO can induce the eastward propagation [24,25]. As inspired by the observed multi-scale features of the MJO [26], the MJO is considered to be a multi-scale envelope, where high-frequency waves provide an instability source to sustain the MJO [27–36]. When considering the trio-interaction among convective heating, moisture processes, and wave-PBL dynamics of the MJO, the frictionally coupled dynamic moisture (FCDM) model produces robust large-scale characteristics of the observed MJO, including slow eastward propagation of 5 m/s, planetary-scale selection, horizontally coupled Rossby–Kelvin wave structure, and PBL convergence preceding major convection [25,37–40].

In comprehensive numerical simulations such as GCMs, precipitation needs to be parameterized. When considering the moisture process in theoretical models, the Betts–Miller scheme [41,42], especially the simple linear Betts–Miller scheme [43], is often used. In the Betts–Miller scheme, there is one important parameter, the convective adjustment time (CAT). The CAT is used to measure how long it takes for the convection to release convective available potential energy (CAPE). When focusing on moisture processes, the CAT is used to represent the moisture relaxation time, which is considered as the time scale for anomalous precipitation to relax moisture back toward its climatological value. Over the convective region, quasi-equilibrium convective schemes suggest that the vertical structure of the heating actually adapts strongly on a fast time scale to balance the effect of larger-scale circulation [44,45]. In this sense, the CAT can be seen as the adjustment time for convection to respond to a departure from the "quasi-equilibrium" state in the atmospheric moisture field [46].

The role of CAT in modeling the MJO in GCMs has been discussed by Jiang et.al. [46], who demonstrated that the effect of CAT is correlated with the model's capability to simulate the MJO. In the FCDM theoretical model for the MJO, the CAT longer than 10 h is the key to simulate the MJO-like frequency; otherwise, the moist Kelvin wave-like dispersion relationship would be simulated [37]. In all these simulations by GCMs or theoretical models including the "moisture mode" model [20,21,23,24], multi-scale interaction model [18,29], and FCDM model [37–39], a spatially uniform CAT is used. The observed CAT, however, has been found to have a spatial distribution in recent observations [47]. The spatial distribution of the reciprocal of the CAT, i.e., the convective relaxation frequency (CRF), is nearly identical to the climatological-mean precipitation [47]. Thus, it is necessary to investigate how the spatial variation of the CAT affects the MJO. To address this scientific question, the aforementioned theoretical FCDM model is used in this work, which has produced robust large-scale characteristics of the MJO [37,38].

The rest of this paper is organized as follows. We describe the FCDM model, the datasets and methods of analysis, and the observational spatial distribution of CAT, in Section 2. We present the role of spatially uniform CAT on the MJO in Section 3, and discuss the role of spatially varying CAT on the MJO in Section 4. Concluding remarks are given in Section 5.

2. Model Framework, Methods and Datasets

2.1. FCDM Model

To investigate the effect of CAT on the MJO, the theoretical FCDM model for the MJO [37,38] is used. This model focuses on the lower-tropospheric dynamics represented by the trio-interaction of diabatic heating-wave dynamics, moisture dynamics, and PBL dynamics. The framework of this model is based on the original Matsuno–Gill model [15,16], augmented by moisture processes. To focus on low-frequency Kelvin and Rossby waves, the longwave approximation is used. In this work, we only discuss the linear processes, while the nonlinear advection terms and the role of the mean flow are all neglected. The strong Rayleigh damping only decreases the growth rate systematically, and therefore

is neglected here. In this moisture equation, the convection in the model consumes moisture q through precipitation P_r, i.e., $q_t \approx -P_r$. The PBL moisture convergence w_b provides a moisture source for the troposphere, i.e., $q_t \approx w_b$. Following the work of Majda and Stechmann [29], only the first baroclinic mode associated with deep convection is studied, and both diabatic heating and vertical velocity anomalies have a vertical structure of $\sin(z)$; thus, the vertical structure for horizontal velocity and geopotential height anomalies is $\cos(z)$. z ranges from 0 at the top of the PBL (900 hPa) to π at the top of the troposphere (100 hPa). The PBL convergence is calculated from a well-mixed PBL, in which the movement is driven by the lower-tropospheric pressure anomaly ϕ. Details of this PBL moisture convergence calculation can be found in Liu and Wang [18,37].

The reference gravity wave speed is given by $C = 50$ ms^{-1}. The temporal and spatial scales are $\sqrt{1/C\beta} = 8.5$ h and $\sqrt{C/\beta} = 1500$ km, respectively, where $\beta = 2.3 \times 10^{-1}$m^{-1}s^{-1} to represent the equatorial curvature effect of the Earth to the first order. The non-dimensional FCDM model can be written for the first baroclinic mode:

$$\begin{aligned} u_t - yv &= -\phi_x, \\ yu &= -\phi_y, \\ \phi_t + (u_x + v_y) - w_b &= -P_r - \mu\phi, \\ q_t + \overline{Q}(u_x + v_y) - \overline{Q}_b w_b &= -P_r, \\ w_b &= d(d_1\phi_{yy} + d_2\phi_y), \end{aligned} \tag{1}$$

where u and v are the zonal and meridional winds, respectively; ϕ is geopotential anomaly; P_r stands for diabatic heating of deep convection associated with precipitation; w_b is vertical velocity caused by the PBL Ekman pumping; and $\mu = 0.18$ is the non-dimensional coefficient for the Newtonian cooling with a time scale of two days. The parameter $\overline{Q}$ is the non-dimensional background vertical moisture gradient (BVMG) in the troposphere, with $\overline{Q} = 0.9$ as the standard value over the SST of 29.5 °C; and $\overline{Q}_b = 1.6$ is the value for the PBL. Both moisture gradients are the largest at the equator and decay poleward with an e-folding damping scale of 30°, associated with the SST structure in Kang et al. [48]. The non-dimensional PBL depth of 100 hPa is represented by $\mu = 0.25$. The PBL Ekman pumping coefficients are $d_1 = E/(E^2 + y^2)$ and $d_2 = -2Ey/(E^2 + y^2)^2$, where $E = 1.1$ is the Ekman number with a time scale of 8 h in the PBL. Details of this model can be found in Liu et al. [37] and in Wang and Chen [38].

In this model, precipitation is parameterized. We adopt a simplified Betts–Miller relaxation-type parameterization [41–43], which can be written as

$$P_r = \frac{1}{\tau}(q + \alpha\phi), \tag{2}$$

where α is the coefficient of reference moisture profile measuring relative contribution of the environmental buoyancy to the CAPE parameterization. Sensitivity experiments showed that the model results are not sensitive to this parameter [37]. In this work, we only focus on the moisture feedback; this process can be neglected by setting $\alpha = 0$. In this theoretical work, only the linear precipitation assumption is considered. The nonlinear precipitation, or positive-only precipitation, which was found to contribute to the planetary-scale selection of the MJO [40,49] and change the horizontal structure of the MJO [50], is not included.

The CAT is denoted by τ, which determines the strength of precipitation response to anomalous moisture. A small τ implies intense cumulus activity is associated with a rapid atmospheric adjustment toward the reference quasi-equilibrium state [44]. Based on the observed precipitation–moisture curve for each grid over the tropics, an averaged value of 13.7 h was obtained [24], which has a non-dimensional value of $\tau = 1.7$.

In the linear FCDM model with spatially uniform CAT, the analytical solution can be obtained by solving the complex eigenvalue problem. For zonally propagating waves, the variables are assumed to

have a structure of $e^{i(kx-\sigma t)}$, where σ is the frequency and k is the wavenumber. Then, phase speed and growth rate can be calculated by $Re(\sigma)/k$ and $Im(\sigma)$, respectively. After projecting the FCDM model on the frequency-wavenumber space, the linear matrix for the five predicted variables in Equation (1), i.e., u, v, w_b, ϕ and q is obtained, and their eigenvalues and eigenvectors are calculated through matrix inversion. Following the work of Majda and Stechmann [29], the simple parabolic cylinder function is used to expand the meridional structure. For simplicity, only the first three lowest meridional modes are used, which have the structures of $\exp(-y^2/2)$, $\exp(-y^2/2)$, and $(2y^2-1)\exp(-y^2/2)$.

When the CAT has a spatially varying distribution, the FCDM model has no analytical solutions, and its solution can only be calculated numerically by integrating the model from specified initial and boundary conditions with appropriate difference schemes. The second-order forward finite difference method is adopted in space, with a spatial step of 2.5° by 2.5°. A typical fourth-order Runge–Kutta scheme with a temporal step of 2.5 min is used for the time integration. Since only the linear processes are included in this work, the results are not sensitive to these schemes. A zonally periodic boundary condition is used for the band from 35° S to 35° N, and no fluxes of mass, momentum, and heat are applied at the meridional boundaries. Simulations are initialized by the pressure perturbation with a Kelvin wave-like structure of $\varphi = \varphi_0(2\pi k_i x/L)$, where L is the non-dimensional circumference of the Earth at the equator, and k_i is the wavenumber of the initial disturbance. In this linear FCDM model, the MJO-like solution will arise naturally for any types of initial perturbation, although it will take different times for the model to reach a steady evolution. The initialization of the MJO controlled by many processes is beyond the capability of this linear FCDM model; thus, we only use this simple Kelvin wave-like initial perturbation in this work. Details of these eigenvalue and initial problems are given by Liu and Wang [25].

2.2. Data

This study uses the daily air temperature and monthly specific humidity from 1000 to 100 hPa, which are obtained from the European Centre for Medium-Range Weather Forecasts (ECMWF) reanalysis-interim (ERA-interim) [51]. Air temperature is used to calculate the saturation column water vapor, and specific humidity is used to calculate the BVMG. Both fields have a horizontal resolution of 1.5° × 1.5°, and the temporal coverage is from 1998 to 2011. Daily averaged precipitation from the 3B42 version-7 product of the Tropical Rainfall Measurement Mission (TRMM-3B42) [52] during the period 1998–2011 is also used in this study. To facilitate comparison with the ERA-interim data and reduce errors resulting from missing observation in space, the TRMM-3B42 dataset is interpolated to 1.5° × 1.5° grid, and then used to calculate the CAT.

2.3. Spatial Distribution of CAT

According to the definition of CAT in Adames [47], the background CAT $\overline{\tau_c}$ can be written in the following form:

$$\overline{\tau_c} = \frac{\langle \overline{q_s} \rangle}{\eta \overline{P_r}}, \tag{3}$$

where $\overline{P_r}$ denotes precipitation, and $\overline{q_s}$ is the saturation water vapor. A value of η = 12.1 is used, which is obtained from a nonlinear least squares fit of TRMM $\overline{q_s}$ and $\overline{P_r}$ at each grid across the Warm Pool (60° E–180° E, 10° S–10° N) [47]. The overbar denotes background mean represented by 100-day low-pass filtering, and the angle bracket denotes the mass-weighted vertical integral of the anomaly field. The column saturation water vapor takes the following form:

$$\langle \overline{q_s} \rangle = \frac{1}{g} \int_{100hPa}^{1000hPa} \overline{q_s} dp. \tag{4}$$

To compare to the background precipitation $\overline{P_r}$, a CRF, i.e., $\overline{v_c}$, which is the reciprocal of CAT, is defined.

The horizontal distributions of climatological mean TRMM 3B42 precipitation $\overline{P_r}$, column saturation column water vapor $\langle \overline{q_s} \rangle$, convective relaxation frequency $\overline{v_c}$, and tropospheric BVMG $\overline{Q}$ are shown in Figure 1. We can see that $\overline{v_c}$ has a nearly identical pattern as the climatological-mean precipitation (Figure 1a,c), which has the maximum value over the equator and decays poleward. This is due to $\langle \overline{q_s} \rangle$ exhibiting relatively little variation in the tropics (Figure 1b), and $\overline{v_c}$ being determined by changes in precipitation. In addition, the distributions of $\overline{v_c}$ and tropospheric BVMG $\overline{Q}$ also bear much resemblance to that of SST (Figure 1d), with larger (smaller) CRF and BVMG over the region where SST is warmer (cooler). The BVMG in the PBL also has the same horizontal structure as the tropospheric BVMG, although its amplitude is 1.8 times the tropospheric one. This figure indicates that the value of CAT is small over climatologically rainy regions and is large over the climatologically dry regions. This observed spatial CAT distribution and its effect on the MJO will be discussed in Section 4.

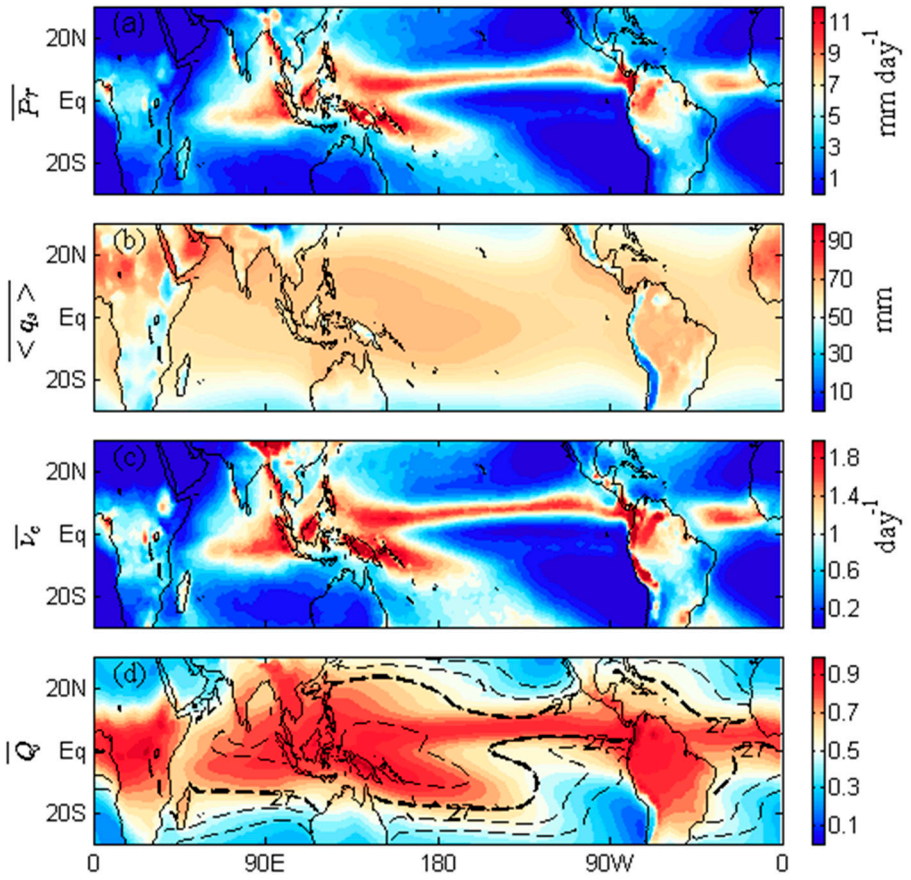

Figure 1. Climatological mean states. Spatial distributions of annual mean: (**a**) TRMM 3B42 precipitation $\overline{P_r}$ (mm day^{-1}); (**b**) column saturation water vapor $\langle \overline{q_s} \rangle$ (mm) from ERA-interim; (**c**) calculated convective relaxation frequency (CRF, day^{-1}) defined by $\overline{v_c} = \eta \overline{P_r} / \langle \overline{q_s} \rangle$; and (**d**) non-dimensional tropospheric (900–1000 hPa) background vertical moisture gradient (BVMG) $\overline{Q}$ from ERA-interim, overlaid by SST from ERA-interim. The thick dashed contour denotes the SST of 27 °C, and the contour interval is 2 °C. For consistency, all data have been interpolated to 1.5° × 1.5° grid. Adapted from Figure 2 of Adames [47].

3. Spatially Uniform CAT

To understand the effect of CAT on the MJO, we first focus on the case of a spatially uniform CAT. With a CAT value of 1 day, the large-scale characteristics of the MJO can be well simulated by this FCDM model [37]; thus, the role of CAT can be studied by calculating the analytical solution for other

spatially uniform values of the CAT. The frequencies of these eastward-propagating modes for different CAT values are shown in Figure 2a. For quick moisture adjustment, e.g., CAT shorter than 10 h, only wavenumber one stays in the intraseasonal range. The short waves with wavenumber larger than one, however, all propagate fast, with periods shorter than 30 days. In addition, the frequency increases with increasing wavenumber, which implies that a moist Kelvin wave-like solution is simulated. For a fixed wavenumber, the frequency grows with decreasing CAT and only the short waves are mostly affected. However, for a CAT value of 12 h, a wavelength-independent dispersion relationship is simulated, and the wavenumbers one to six all stay in the MJO frequency range with periods between 30 and 90 days. For a very slow convective adjustment process with CAT longer than 2 days, the frequency is very small and all wavenumbers have periods longer than 90 d. The effect of spatially uniform values of the CAT on the growth rate is shown in Figure 2b. For different values of CAT, the growth rate always decreases with increasing wavenumber, which means that the planetary-scale selection in terms of instability caused by the PBL Ekman pumping always exists in the FCDM model. The unstable modes mainly occur from wavenumber one to wavenumber two, and the growth rate becomes small when the CAT value becomes large. Wavenumber one becomes damped when the CAT is longer than 2 days, and wavenumber two becomes damped when the CAT is longer than 5 h (not shown). This result means that a large value of CAT and a slow convective adjustment process will damp the instability caused by the PBL Ekman pumping. In GCM simulations, the MJO strength is also suppressed when the value of CAT is increased [46]. Different from the traditional Matsuno–Gill theory with a Kuo-type precipitation parameterization [15,16,38], in which the frequency of convectively coupled equatorial waves increases with a drier mean state and larger moist static stability, the moisture process introduces a new solution in the FCDM model [37], and the long CAT decreases both frequency and growth rate.

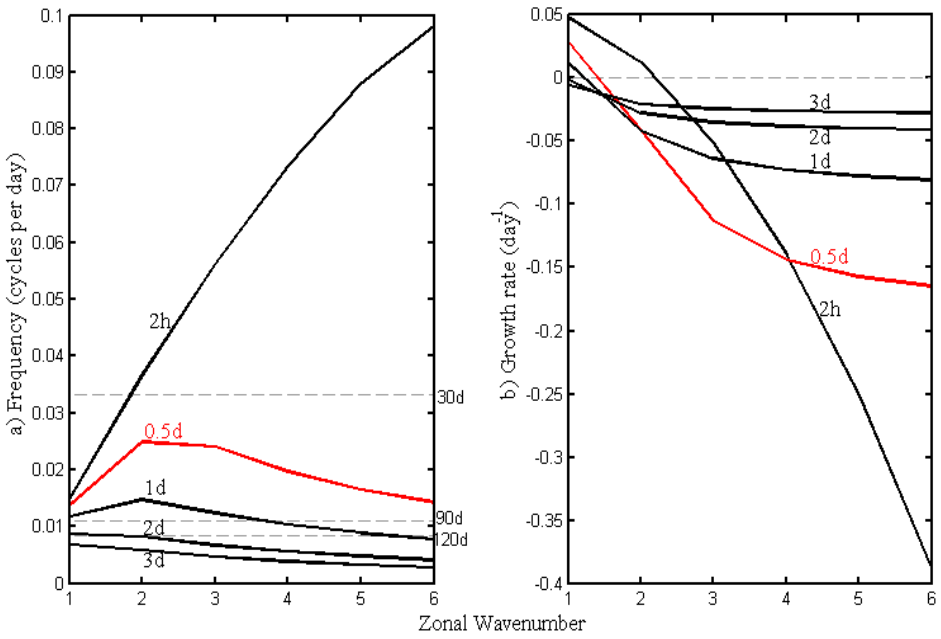

Figure 2. Sensitivity of FCDM model to different values of convective adjustment time (CAT): (**a**) frequency (cycles per day); and (**b**) growth rate (day^{-1}) as a function of wavenumber with different CAT values of 2 h, 0.5, 1, 2, and 3 days in the FCDM model.

The solution of the FCDM model simulates the horizontal Rossby–Kelvin wave structure for different CAT values (Figure 3). A low-pressure anomaly leads a convective center to the east with a phase lag less than $\pi/4$, flanked by an anticyclonic pair. The small phase lag between the negative pressure anomaly and positive diabatic heating associated with precipitation can provide positive

CAPE for the eastward-propagating mode to grow. The upward PBL Ekman pumping also leads the convective center to the east, which tends to moisten the lower troposphere and precondition the occurrence of deep convection. The modulation of the CAT on the horizontal structure of eastward-propagating wavenumber one is also shown in Figure 3. When the CAT changes, two main changes occur: the phase lag between the PBL Ekman pumping and convective center, and the amplitude difference between the Rossby component and the Kelvin component. When the value of CAT is large, the phase lag between the PBL Ekman pumping and convective center increases, which means after the moistening by the PBL, the occurrence of deep convection is delayed by a slow convective adjustment process. Meanwhile, the Rossby component in this Kelvin–Rossby wave system increases as the CAT value increases. The situation is opposite when the value of CAT is small.

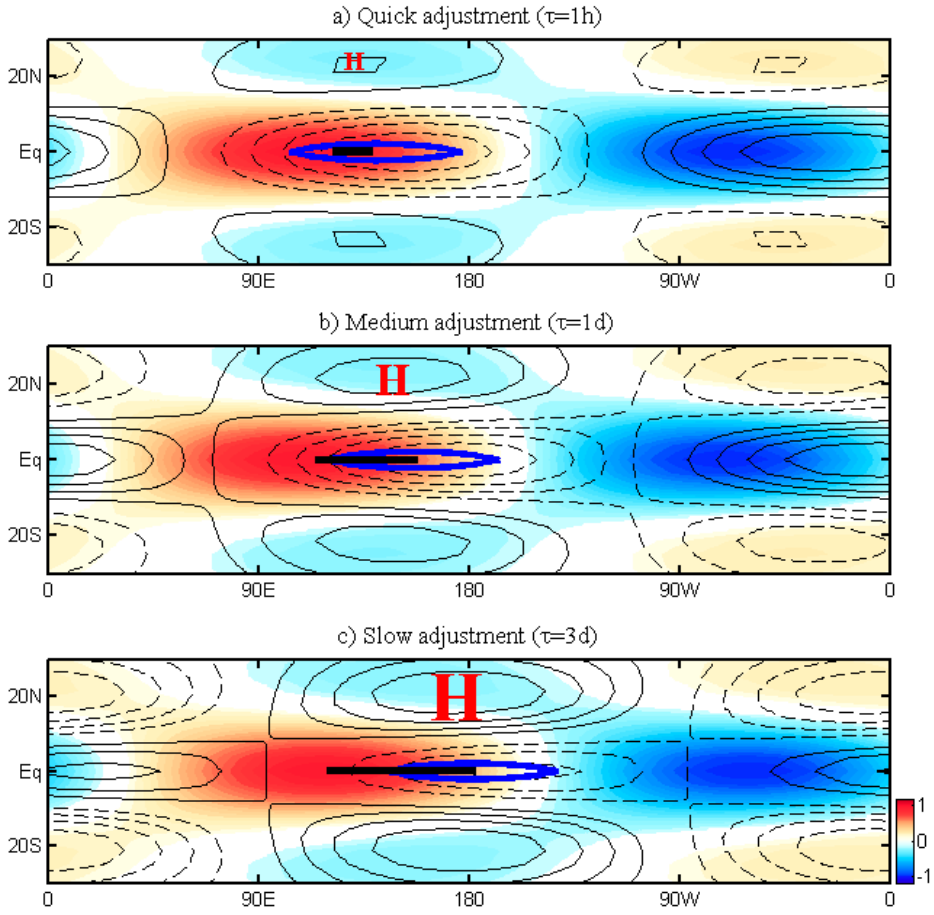

Figure 3. Horizontal structures of the eastward-propagating wavenumber-1 mode associated with different values of the spatially uniform CAT. Shown are normalized precipitation anomalies (shading) as well as contours of lower-tropospheric pressure anomalies for different CAT values of (**a**) τ = 1 h, (**b**) τ = 1 d, and (**c**) τ = 3 d. Positive (negative) anomalies are denoted by solid (dashed) lines. The contour interval is one-fifth of the maximum, and zero contour is not shown. The 0.8 amplitude of the upward PBL Ekman pumping (thick blue contour) is also shown. The thick black lines connect the centers of the convection and PBL moisture convergence. The red "H" denotes the subtropical high pressure center with its font size roughly proportional to the pressure anomaly strength.

In this coupled Kelvin–Rossby wave system, the Kelvin wave contributes to the eastward propagation while the Rossby wave contributes to the westward propagation. The horizontal structure, especially the relatively strength of the Kelvin and Rossby components, will determine the propagation direction of this coupled system. Thus, we use the Rossby–Kelvin amplitude ratio to identify these

relative roles of Kelvin and Rossby waves. The role of moisture advection, which leads to the eastward propagation of the MJO [24,53], is not included in this work. Figure 4a,b shows the modulation effects of CAT on the Ekman pumping-convective center phase lag and Rossby–Kelvin amplitude ratio of different wavenumbers, respectively. The phase lag between the upward Ekman pumping and convective center is usually larger for the short waves than for the long waves. When the value of CAT becomes large, the phase lag increases, and this phase lag increase is much larger for the short waves than for the long waves. For a long CAT of 3 days, the upward PBL Ekman pumping leads the convective center by a phase lag of more than $\pi/2$, which means the occurrence of deep convection is strongly delayed and the upward Ekman pumping is closer to the negative convective center than to the positive convective center; thus, the positive temperature anomaly or negative pressure anomaly has small projection on the positive diabatic heating, resulting in negative CAPE. In general, the short waves have a stronger Rossby component than the long waves, and the Rossby component is enhanced when the CAT value becomes large. This Rossby component enhancement is robust for the short waves while it has less effect on the long waves. Since both the delay of deep convection occurrence and strong westward-propagating Rossby component can slow down the eastward propagation of this coupled system, the eastward propagation of short waves will be significantly slowed down when the value of CAT becomes large.

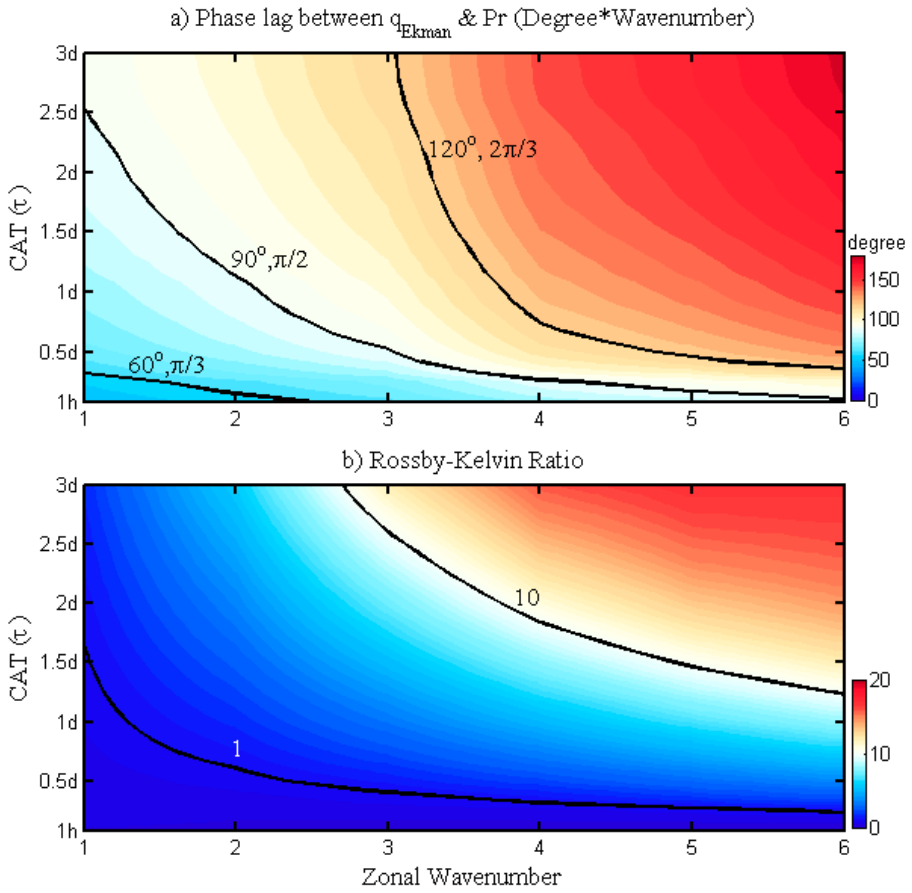

Figure 4. Phase lag and Rossby–Kelvin ratio associated with different values of spatially uniform CAT: (**a**) phase lag between upward PBL Ekman pumping and precipitation on the equator; and (**b**) Rossby–Kelvin ratio as a function of wavenumber and spatially uniform CAT in the FCDM model. Phase lag for all waves is compared in a range of 360 degrees by multiplying the wavenumber. The Rossby–Kelvin ratio is defined by the ratio of the maximum pressure anomalies between the off-equatorial (15°–20° N) and equatorial (5° S–5° N) regions.

In the observations (Figure 1), the value of CAT is small or the convective adjustment process is quick over warm SST associated with large BVMG $\overline{Q}$ and $\overline{Q}_b$ in the troposphere and PBL, respectively. For the instability caused by the PBL moisture convergence, previous work showed that the frequency is increased and the growth rate is decreased when the SST becomes cold [25,37]. This result can also be seen in Figure 5, and the change mainly occurs for short CAT.

In the observations of the MJO [5], its phase speed remains the same over the Indo-Western Pacific region where the convection and circulation of the MJO are well coupled. In Figure 5a, a scatterplot of tropospheric BVMG and CAT in the Warm Pool illustrates that the BVMG and CAT stay along the line where the frequency and phase speed for wavenumber one are nearly the same. The observations show that for cold SSTs, the BVMG is small while the CAT value is large (Figure 1). The low BVMG associated with a stable troposphere will increase the frequency, while the long CAT will decrease the frequency. The correlation between BVMG and CAT over each longitude is 0.75. Thus, these positive and negative feedbacks counteract against each other, leaving both frequency and phase speed less affected (Figure 5a). This provides a new mechanism for explaining why the phase speed of the MJO remains the same over the Indo-Western Pacific region.

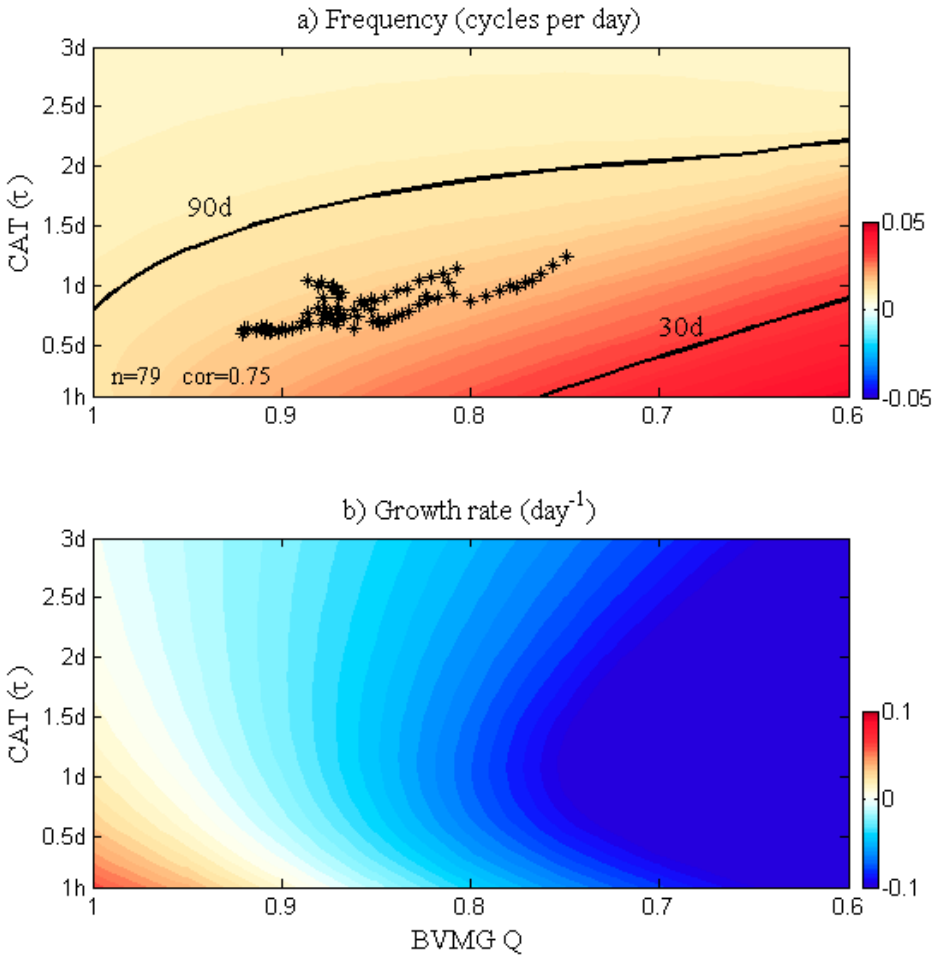

Figure 5. Effects of spatially uniform CAT and tropospheric BVMG on eastward-propagating wavenumber one: (**a**) frequency (cycles per day); and (**b**) growth rate (day^{-1}) as a function of BVMG and spatially uniform CAT for wavenumber one in the FCDM model. The frequencies associated with periods of 30 and 90 d are indicated for references. A scatterplot of calculated band-averaged (10° S–10° N) CAT vs. tropospheric BVMG in Figure 1 over the Indo-Pacific Ocean from 60° E to 180° E is also represented by the black asterisk in (**a**). The sample number is 79, and the correlation between the CAT and BVMG is 0.75.

4. Warm Pool-Like CAT

A large value of CAT is found to slow down the eastward propagation and reduce the growth rate of the MJO through delaying the convection (Figures 2 and 4). Previous works also showed that the small BVMG in the troposphere and the PBL deceases the growth of the MJO through increasing the gross moist stability in the troposphere and decreasing the PBL moisture convergence [37,48]. The role of spatially non-uniform CAT in MJO evolution can be studied by integrating the model from an initial perturbation. Since the CRF (reciprocal of CAT) is maximum over the Warm Pool region and decays poleward (Figure 1c), we can use an idealized Warm Pool-like structure to represent a spatially non-uniform CAT (Figure 6a). The idealized Warm Pool-like BVMG in the troposphere and the PBL is also used to represent the mean state of moisture distribution (Figure 6b). Four experiments are carried out to study the effect of spatially non-uniform CAT on the MJO, as well as the coupled role of spatially non-uniform BVMG. Exp 1 with zonally uniform CRF (or CAT) and BVMG is run first as a reference. In Exp 2, zonally uniform CRF and Warm Pool-like BVMG are used to study the role of spatially non-uniform BVMG. In Exp 3, zonally uniform BVMG and Warm Pool-like CRF are used to study the role of spatially non-uniform CRF. In Exp 4, a Warm Pool-like structure is used for both BVMG and CRF to study the combined role of spatially non-uniform BVMG and CRF. In all four experiments, a wavenumber-one Kelvin wave-like initial perturbation is used.

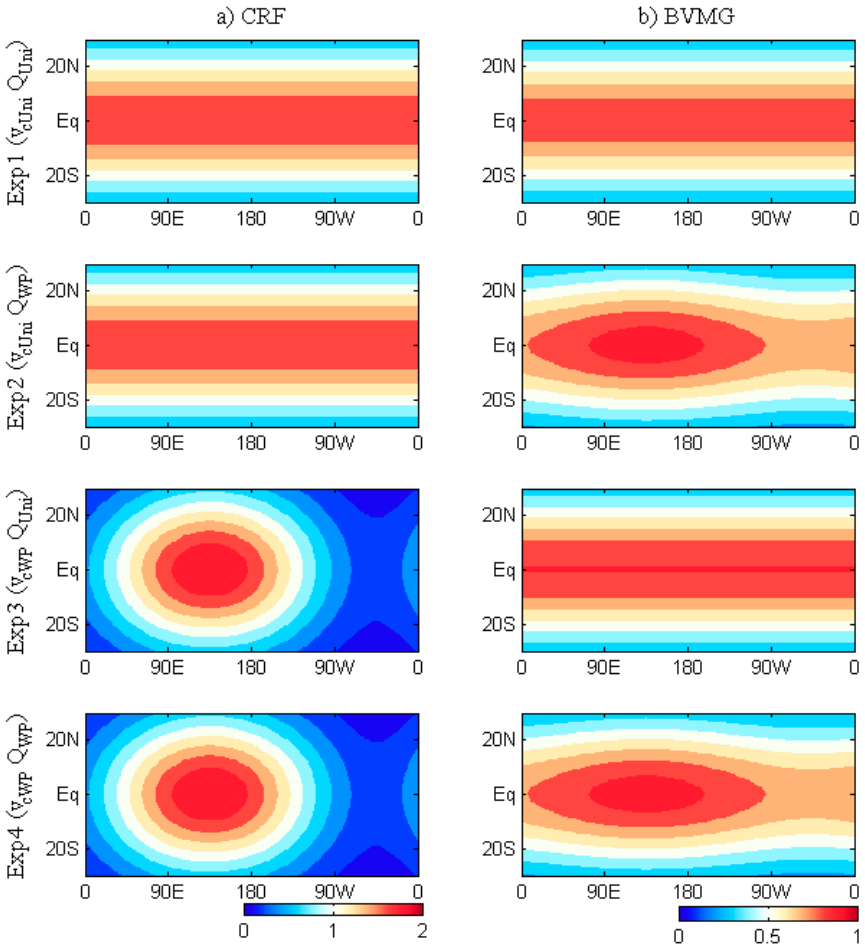

Figure 6. Mean states of four sensitivity experiments: (**a**) the CRF (day^{-1}); and (**b**) the non-dimensional tropospheric BVMG used in the four experiments (Exp 1, Exp 2, Exp 3, and Exp 4). In Exp 1, zonally uniform CRF and BVMG are used, while the Warm Pool-like mean state is used in Exp 4. In Exp 2 and Exp 3, the zonally uniform and Warm Pool-like pattern are used for these two fields, respectively.

In Exp 1 with zonally uniform mean state, the model result reaches a steady state after an adjustment of 5 days (Figure 7a). Over the uniform SST of 29.5 °C, the standard tropospheric BVMG is 0.9, and the CAT is 13.7 h. This steady solution propagates eastward with a phase speed of 7.1 m/s. In Exp 2 with Warm Pool-like BVMG (Figure 7b), the convection mainly prevails over the Warm Pool region, and is suppressed over the cold SSTs. The phase speed of this eastward propagation is about 5 m/s over the Warm Pool region, while the wavenumber-one mode propagates eastward very fast over the cold SSTs, since the phase speed of moist Kelvin waves increases quickly with small moist static energy [54]. In Exp 3 with a Warm Pool-like CRF, a similar evolution as that in Exp 2 is simulated, and the convection mainly prevails in the Warm Pool region and decays quickly over the cold SSTs (Figure 7c). Different from Exp 2 in which the eastward propagation becomes fast after reaching the cold SST region, the phase speed does not change too much over the small CRF (or long CAT) region where the convection is suppressed in Exp 3. In Exp 4, where both Warm Pool-like BVMG and CRF are used, the convection is strongly confined in the Warm Pool region. Outside the Warm Pool region, both small BVMG and long CAT reduce the growth rate and suppress the convection. The phase speed over the Warm Pool region in Exp 4 remains the same as in Exp 3, which mimics the observations very well [5]. For some successive MJO events, a weak circumnavigating signal in column-integrated latent heating can be found in Version 2 of the NASA Modern Era Reanalysis for Research and Applications (MERRA-2) reanalysis [55], which has a similar evolution between Exp 2 and Exp 4.

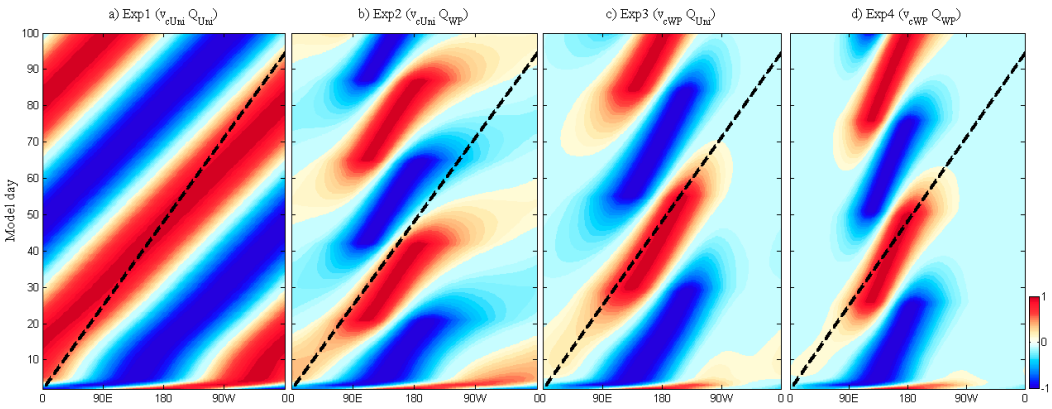

Figure 7. Zonal propagation changed by using different mean states. Hovemöller plots of normalized equatorial precipitation in: (**a**) Exp 1; (**b**) Exp 2; (**c**) Exp 3; and (**d**) Exp 4. The dashed line shows the reference speed of 5 m/s. The equatorial precipitation of each day is normalized by its maximum value.

The horizontal structures simulated in these four experiments are shown in Figure 8. The coupled Kelvin–Rossby system is simulated in all four experiments. The convective center is led by easterly wind anomalies to the east, which is favorable for the upward PBL Ekman pumping to transfer moisture into the troposphere and precondition deep convection. For the zonally uniform mean state in Exp 1, a symmetric solution is simulated (Figure 8a). For a Warm Pool-like BVMG, the convection only prevails over the Warm Pool region and is suppressed in the cold tongue region (Figure 8b). Similar horizontal structure as in Exp 2 is also simulated in Exp 3 with a Warm Pool-like CAT, and the zonal scales of convection and circulation are relatively smaller than those in Exp 1 (Figure 8c). When the Warm Pool-like structure is used for both BVMG and CAT in Exp 4 (Figure 8d), the convection and circulation are both confined in the Warm Pool region and their zonal scales become even smaller. The convection over the cold tongue region is heavily suppressed. Compared to the wavenumber-one structure in Exp 1, the zonal structures become small when the Warm Pool-like mean state is used in Exp 2–Exp 4. Figure 2a shows that all short waves propagate eastward more slowly than wavenumber one; thus, the convection in Exp 2–Exp 4 should have slower eastward propagation than that in Exp 1 (Figure 7).

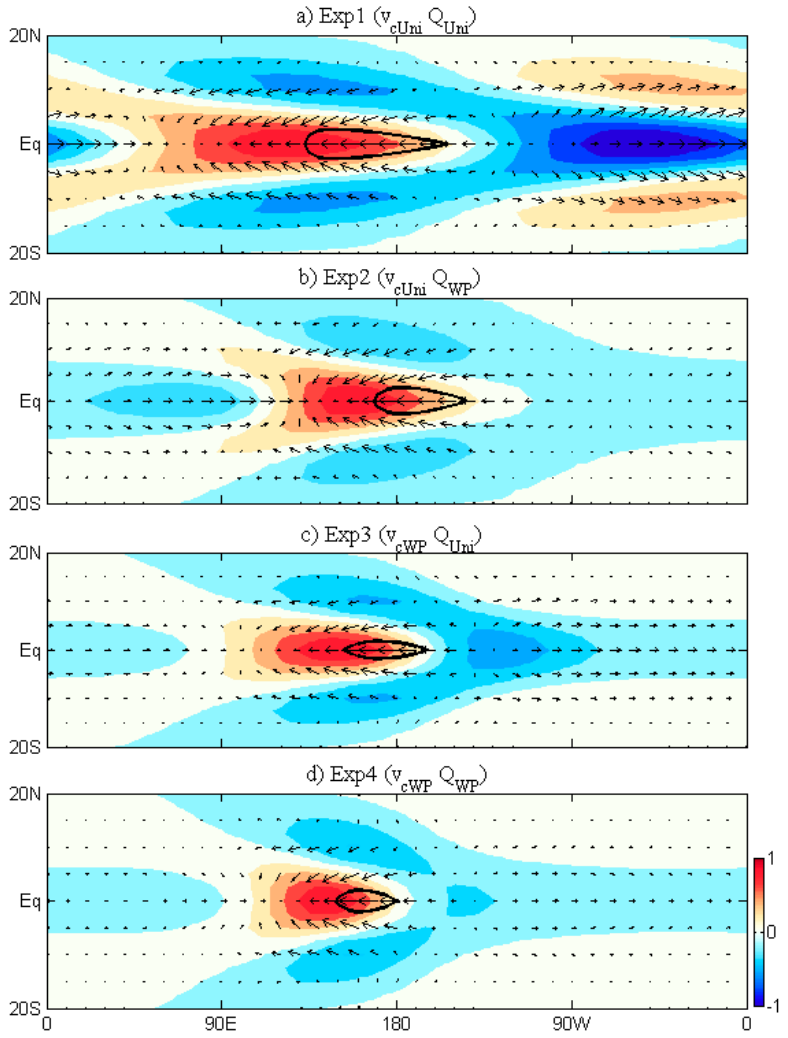

Figure 8. Horizontal structures in different experiments. Shown are normalized precipitation (shading) and lower-level wind (vector) at day 30 in: (**a**) Exp 1; (**b**) Exp 2; (**c**) Exp 3; and (**d**) Exp 4. The 0.8 amplitude of the upward PBL Ekman pumping (thick black contour) is also shown.

5. Concluding Remarks

In the most current MJO theories that focus on moisture processes [20–22,24,25,37,38], the CAT is a key parameter that helps determine the relationship between MJO precipitation and column moisture. Recent observations [47] reveal that the CAT of the MJO exhibits significant spatial variation: It is long over regions where climatological mean precipitation is small (Figure 1). By using the theoretical FCDM model for the MJO, our results show that a large value of CAT decreases the frequency and growth rate of eastward-propagating MJO-like mode in the FCDM model (Figure 2). The main reason is that a large value of CAT delays the occurrence of deep convection of the MJO, resulting in slow eastward propagation and large phase lag between circulation and convection (Figures 3 and 4). This large phase lag decreases the CAPE and reduces the growth rate. The Rossby component is also enhanced when the CAT becomes long, which also helps to slow down the eastward propagation.

In the observations, the value of CAT is usually large when the BVMG is low or the SST is cold (Figure 1). Since the long CAT decreases the frequency while the low BLMG increases the frequency through reducing the tropospheric moist static energy, the frequency or phase speed remains the same when the BVMG becomes small while the value of CAT becomes large (Figure 5a). Under the Warm Pool-like BVMG and CAT mimicking the observations, the simulated eastward propagation in the

FCDM model also has the same speed along the equator in the Indo-Western Pacific region (Figure 7d), which is consistent with the observations of the MJO [5]. The simulated convection prevails over the Warm Pool region and becomes very weak over the cold SSTs (Figure 7d), since both small BVMG and long CAT over the cold SST region tend to reduce the growth rate and suppress the convection of the MJO. This result explains why the MJO is suppressed over the long CAT region in the observations [47] and why the value of CAT is correlated with the model's capability to simulate the MJO [46].

The theoretical work presented in this study highlights many important aspects of the MJO and helps improve our understanding of the MJO dynamics in the real world. As one of the "self-similarity" systems [56], the transition from shallow to deep convection has been found to be a key process for the MJO [57]. The MJO is preceded by shallow convection to its east [57–59]. In this work, only the first baroclinic mode is included. The multi-cloud interaction in the MJO, represented by the first and second baroclinic mode [28,60], is not included. This transition from shallow to deep convection, however, can be parameterized by slow adjustment process, and a long CAT means weak transition, i.e., strong shallow convection and weak deep convection. The important effect of spatially varying CAT on the MJO demonstrates the importance of precipitation parameterization in GCM simulations of MJO, especially the different ratios of shallow to deep convection should be correctly captured.

Acknowledgments: This work was supported by the China National 973 Project (2015CB453200), the National Natural Science Foundation of China (41420104002), the IPOVAR Project (GASI-IPOVAI-02), and the Natural Science Foundation of Jiangsu Province (BK20150907). This paper is ESMC Contribution No. 191.

Author Contributions: Fei Liu conceived and designed the numerical experiments; Hui Wang and Yuntao Wei analyzed the observational data and performed the numerical experiments, respectively. All authors wrote, drafted and revised this article.

Conflicts of Interest: The authors declare no conflict of interest.

References

1. Madden, R.A.; Julian, P.R. Detection of a 40–50 day oscillation in the zonal wind in the tropical pacific. *J. Atmos. Sci.* **1971**, *28*, 702–708. [CrossRef]
2. Madden, R.A.; Julian, P.R. Description of global-scale circulation cells in the tropics with a 40–50 day period. *J. Atmos. Sci.* **1972**, *29*, 1109–1123. [CrossRef]
3. Zhang, C. Madden–Julian oscillation: Bridging weather and climate. *Bull. Am. Meteorol. Soc.* **2013**, *94*, 1849–1870. [CrossRef]
4. Waliser, D.E.; Moncrieff, M.W.; Burridge, D.; Fink, A.H.; Gochis, D.; Goswami, B.N.; Guan, B.; Harr, P.; Heming, J.; Hsu, H.H. The "year" of tropical convection (May 2008–April 2010): Climate variability and weather highlights. *Bull. Am. Meteorol. Soc.* **2012**, *93*, 1189–1218. [CrossRef]
5. Zhang, C. Madden-julian oscillation. *Rev. Geophys.* **2005**, *43*, 453–468. [CrossRef]
6. Donald, A.; Meinke, H.; Power, B.; Maia, A.D.H.N.; Wheeler, M.C.; White, N.; Stone, R.C.; Ribbe, J. Near-global impact of the Madden-Julian Oscillation on rainfall. *Geophys. Res. Lett.* **2006**, *33*, 72–88. [CrossRef]
7. Jiang, X.; Waliser, D.E.; Xavier, P.K.; Petch, J.; Klingaman, N.P.; Woolnough, S.J.; Guan, B.; Bellon, G.; Crueger, T.; Demott, C. Vertical structure and physical processes of the Madden-Julian Oscillation: Exploring key model physics in climate simulations. *J. Geophys. Res. Atmos.* **2015**, *120*, 4718–4748. [CrossRef]
8. Charney, J.G.; Eliassen, A. On the growth of the hurricane depression. *J. Atmos. Sci.* **1964**, *21*, 68–75. [CrossRef]
9. Lindzen, R.S. Wave-cisk in the tropics. *J. Atmos. Sci.* **1974**, *31*, 156–179. [CrossRef]
10. Lau, K.; Peng, L. Origin of low-frequency (intraseasonal) oscillations in the tropical atmosphere. Part I: Basic theory. *J. Atmos. Sci.* **1987**, *44*, 950–972. [CrossRef]
11. Chang, C.P.; Lim, H. Kelvin wave-cisk: A possible mechanism for the 30–50 day oscillations. *J. Atmos. Sci.* **1988**, *45*, 1709–1720. [CrossRef]
12. Emanuel, K.A.; David Neelin, J.; Bretherton, C.S. On large-scale circulations in convecting atmospheres. *Q. J. R. Meteorol. Soc.* **1994**, *120*, 1111–1143. [CrossRef]

13. Hayashi, Y.; Golder, D. United mechanisms for the generation of low-and high-frequency tropical waves. Part I: Control experiments with moist convective adjustment. *J. Atmos. Sci.* **1997**, *54*, 1262–1276. [CrossRef]
14. Wang, B. Dynamics of tropical low-frequency waves: An analysis of the moist kelvin wave. *J. Atmos. Sci.* **1988**, *45*, 2051–2065. [CrossRef]
15. Matsuno, T. Quasi-geostrophic motions in the equatorial area. *J. Meteorol. Soc. Jpn.* **1966**, *44*, 25–43. [CrossRef]
16. Gill, A.E. Some simple solutions for heat-induced tropical circulation. *Q. J. R. Meteorol. Soc.* **1980**, *106*, 447–462. [CrossRef]
17. Wang, B.; Rui, H. Dynamics of the coupled moist kelvin-rossby wave on an equatorial β-plane. *J. Atmos. Sci.* **1990**, *47*, 397–413. [CrossRef]
18. Liu, F.; Wang, B. A frictional skeleton model for the Madden-Julian Oscillation. *J. Atmos. Sci.* **2012**, *69*, 2749–2758. [CrossRef]
19. Wang, B.; Li, T. Convective interaction with boundary-layer dynamics in the development of a tropical intraseasonal system. *J. Atmos. Sci.* **1994**, *51*, 1386–1400. [CrossRef]
20. Sobel, A.; Maloney, E. An idealized semi-empirical framework for modeling the Madden-Julian Oscillation. *J. Atmos. Sci.* **2012**, *69*, 1691–1705. [CrossRef]
21. Sobel, A.; Maloney, E. Moisture modes and the eastward propagation of the MJO. *J. Atmos. Sci.* **2013**, *70*, 187–192. [CrossRef]
22. Fuchs, Z.; Raymond, D.J. Large-scale modes in a rotating atmosphere with radiative convective instability and wishe. *J. Atmos. Sci.* **2005**, *62*, 4084–4094. [CrossRef]
23. Fuchs, Ž.; Raymond, D.J. A simple model of intraseasonal oscillations. *J. Adv. Model. Earth Syst.* **2017**, *9*, 1195–1211. [CrossRef]
24. Adames, Á.F.; Kim, D. The mjo as a dispersive, convectively coupled moisture wave: Theory and observations. *J. Atmos. Sci.* **2016**, *73*, 913–941. [CrossRef]
25. Liu, F.; Wang, B. Role of horizontal advection of seasonal-mean moisture in the Madden-Julian Oscillation: A theoretical model analysis. *J. Clim.* **2016**, *29*, 6277–6293. [CrossRef]
26. Nakazawa, T. Tropical super clusters within intraseasonal variations over the western pacific. *J. Meteorol. Soc. Jpn.* **1988**, *66*, 823–839. [CrossRef]
27. Majda, A.J.; Biello, J.A. A multiscale model for tropical intraseasonal oscillations. *Proc. Natl. Acad. Sci. USA* **2004**, *101*, 4736–4741. [CrossRef] [PubMed]
28. Majda, A.J.; Stechmann, S.N.; Khouider, B. Madden-Julian Oscillation analog and intraseasonal variability in a multicloud model above the equator. *Proc. Natl. Acad. Sci. USA* **2007**, *104*, 9919–9924. [CrossRef] [PubMed]
29. Majda, A.J.; Stechmann, S.N. The skeleton of tropical intraseasonal oscillations. *Proc. Natl. Acad. Sci. USA* **2009**, *106*, 8417–8422. [CrossRef] [PubMed]
30. Wang, B.; Liu, F. A model for scale interaction in the Madden-Julian Oscillation. *J. Atmos. Sci.* **2011**, *68*, 2524–2536. [CrossRef]
31. Liu, F.; Wang, B. A model for the interaction between 2-day waves and moist kelvin waves. *J. Atmos. Sci.* **2012**, *69*, 611–625. [CrossRef]
32. Liu, F.; Wang, B. Impacts of upscale heat and momentum transfer by moist kelvin waves on the Madden–Julian Oscillation: A theoretical model study. *Clim. Dyn.* **2013**, *40*, 213–224. [CrossRef]
33. Liu, F.; Huang, G.; Feng, L. Critical roles of convective momentum transfer in sustaining the multi-scale madden–julian oscillation. *Theor. Appl. Climatol.* **2012**, *108*, 471–477. [CrossRef]
34. Yang, D.; Ingersoll, A.P. Testing the hypothesis that the mjo is a mixed rossby-gravity wave packet. *J. Atmos. Sci.* **2011**, *68*, 226–239. [CrossRef]
35. Yang, D.; Ingersoll, A.P. Triggered convection, gravity waves, and the MJO: A shallow water model. *J. Atmos. Sci.* **2013**, *70*, 2476–2486. [CrossRef]
36. Yang, D.; Ingersoll, A.P. A theory of the MJO horizontal scale. *Geophys. Res. Lett.* **2014**, *41*, 1059–1064. [CrossRef]
37. Liu, F.; Wang, B. Effects of moisture feedback in a frictional coupled kelvin–rossby wave model and implication in the Madden–Julian Oscillation dynamics. *Clim. Dyn.* **2016**, *48*, 513–522. [CrossRef]
38. Wang, B.; Chen, G. A general theoretical framework for understanding essential dynamics of Madden-Julian Oscillation. *Clim. Dyn.* **2016**, *49*, 2309–2328. [CrossRef]
39. Wang, B.; Fei, L.; Chen, G. A trio-interaction theory for Madden-Julian Oscillation. *Geosci. Lett.* **2016**, *3*, 34. [CrossRef]

40. Wei, Y.; Liu, F.; Mu, M.; Ren, H.-L. Planetary scale selection of the Madden–Julian Oscillation in an air-sea coupled dynamic moisture model. *Clim. Dyn.* **2017**, 1–16. [CrossRef]
41. Betts, A. A new convective adjustment scheme. Part I: Observational and theoretical basis. *Q. J. R. Meteorol. Soc.* **1986**, *112*, 677–691.
42. Betts, A.; Miller, M. A new convective adjustment scheme. Part II: Single column tests using gate wave, bomex, atex and arctic air-mass data sets. *Q. J. R. Meteorol. Soc.* **1986**, *112*, 693–709.
43. Frierson, D.M.; Majda, A.J.; Pauluis, O.M. Large scale dynamics of precipitation fronts in the tropical atmosphere: A novel relaxation limit. *Commun. Math. Sci.* **2004**, *2*, 591–626. [CrossRef]
44. Neelin, J.D.; Yu, J.-Y. Modes of tropical variability under convective adjustment and the Madden-Julian Oscillation. Part i: Analytical theory. *J. Atmos. Sci.* **1994**, *51*, 1876–1894. [CrossRef]
45. Neelin, J.D.; Zeng, N. A quasi-equilibrium tropical circulation model—formulation. *J. Atmos. Sci.* **2000**, *57*, 1741–1766. [CrossRef]
46. Jiang, X.; Zhao, M.; Maloney, E.D.; Waliser, D.E. Convective moisture adjustment time-scale as a key factor in regulating model amplitude of the Madden-Julian Oscillation. *Geophys. Res. Lett.* **2016**, *43*, 10412–10419. [CrossRef]
47. Adames, Á.F. Precipitation budget of the Madden-Julian Oscillation. *J. Atmos. Sci.* **2017**, *74*, 1799–1817. [CrossRef]
48. Kang, I.-S.; Liu, F.; Ahn, M.-S.; Yang, Y.-M.; Wang, B. The role of sst structure in convectively coupled kelvin–rossby waves and its implications for MJO formation. *J. Clim.* **2013**, *26*, 5915–5930. [CrossRef]
49. Li, T.; Zhou, C. Planetary scale selection of the madden-julian oscillation. *J. Atmos. Sci.* **2009**, *66*, 2429–2443. [CrossRef]
50. Majda, A.J.; Stechmann, S.N. Nonlinear dynamics and regional variations in the MJO skeleton. *J. Atmos. Sci.* **2011**, *68*, 3053–3071. [CrossRef]
51. Dee, D.P.; Uppala, S.M.; Simmons, A.J.; Berrisford, P.; Poli, P.; Kobayashi, S.; Andrae, U.; Balmaseda, M.A.; Balsamo, G.; Bauer, P.; et al. The era-interim reanalysis: Configuration and performance of the data assimilation system. *Q. J. R. Meteorol. Soc.* **2011**, *137*, 553–597. [CrossRef]
52. Huffman, G.A.; Adler, R.; Bolvin, D.T.; Gu, G.; Nelkin, E.; Bowman, K.; Hong, Y.; Stocker, T.; Wolff, D. The trmm multi-satellite precipitation analysis (tmpa): Quasi-global, multiyear, combined-sensor precipitation estimates at fine scale. *J. Hydrometeorol.* **2007**, *8*, 38–55. [CrossRef]
53. Sobel, A.; Wang, S.; Kim, D. Moist static energy budget of the MJO during dynamo. *J. Atmos. Sci.* **2014**, *71*, 4276–4291. [CrossRef]
54. Kiladis, G.N.; Wheeler, M.C.; Haertel, P.T.; Straub, K.H.; Roundy, P.E. Convectively coupled equatorial waves. *Rev. Geophys.* **2009**, *47*, 2003. [CrossRef]
55. Powell, S.W. Successive mjo propagation in merra-2 reanalysis. *Geophys. Res. Lett.* **2017**. [CrossRef]
56. Mapes, B.; Tulich, S.; Lin, J.; Zuidema, P. The mesoscale convection life cycle: Building block or prototype for large-scale tropical waves? *Dyn. Atmos. Oceans* **2006**, *42*, 3–29. [CrossRef]
57. Zhang, G.J.; Song, X. Interaction of deep and shallow convection is key to Madden-Julian Oscillation simulation. *Geophys. Res. Lett.* **2009**, *36*, 269–277. [CrossRef]
58. Benedict, J.J.; Randall, D.A. Observed characteristics of the MJO relative to maximum rainfall. *J. Atmos. Sci.* **2007**, *64*, 2332–2354. [CrossRef]
59. Del Genio, A.D.; Chen, Y.; Kim, D.; Yao, M.-S. The mjo transition from shallow to deep convection in cloudsat/calipso data and giss gcm simulations. *J. Clim.* **2012**, *25*, 3755–3770. [CrossRef]
60. Khouider, B.; Majda, A.J. A simple multicloud parameterization for convectively coupled tropical waves. Part I: Linear analysis. *J. Atmos. Sci.* **2006**, *63*, 1308–1323. [CrossRef]